Icarus xxx (xxxx) xxx

Contents lists available at ScienceDirect

Icarus

journal homepage: www.elsevier.com/locate/icarus

The source of hydrogen in earth's building blocks

Thomas J. Barrett [a,*], James F.J. Bryson [a], Kalotina Geraki [b]

[a] Department of Earth Sciences, University of Oxford, Oxford OX1 3AN, UK
[b] Diamond Light Source, Harwell Science and Innovation Campus, Didcot OX11 0DE, UK

ARTICLE INFO

Keywords:
Meteorites
Planetary formation
Cosmochemistry

ABSTRACT

Despite being pivotal to the habitability of our planet, the process by which Earth gained its present-day hydrogen budget is unclear. Due to their isotopic similarity to terrestrial rocks across a range of elements, the meteorite group that is thought to best represent Earth's building blocks is the enstatite chondrites (ECs). Because of ECs' nominally anhydrous mineralogy, these building blocks have long been presumed to have supplied negligible hydrogen to the proto-Earth. However, recent bulk compositional measurements suggest that ECs may unexpectedly contain enough hydrogen to readily explain Earth's present-day water abundance. Together, these contradictory findings mean the contribution of ECs to Earth's hydrogen budget is currently unclear. As such, it is uncertain whether appreciable hydrogen is a systematic outcome of Earth's formation. Here, we explore the amount of hydrogen in ECs as well as the phase that may carry this element using sulfur X-ray absorption near edge structure (S-XANES) spectroscopy. We find that hydrogen bonded to sulfur is prevalent throughout the meteorite, with fine matrix containing on average almost 10 times more H—S than chondrule mesostasis. Moreover, the concentration of the H—S bond is linked to the abundance of micrometre-scale pyrrhotite ($Fe_{1-x}S$, $0 < x < 0.125$). This sulfide can sacrificially catalyse a reaction with H_2 from the disk at high temperatures to create H_2S, which could be dissolved in adjoining molten silicate-rich material. Upon rapid cooling, this assemblage would form pyrrhotite encased in submicron silicate-rich glass that carries trapped H_2S. These findings indicate that hydrogen is present in ECs in higher concentrations than previously considered and could suggest that this element may have a systematic, rather than stochastic, origin on our planet.

1. Introduction

Although water is central to planetary habitability as we know it, the mechanism by which Earth gained its substantial present-day water budget is unclear. Enstatite chondrites (ECs) closely resemble terrestrial rocks across a range of isotopic compositions (Dauphas, 2017). Hence, ECs (or material similar to these meteorites) have been suggested as the predominant building blocks of the proto-Earth (Javoy et al., 2010), as well as other terrestrial planets including Mars (Brasser et al., 2018). ECs formed in the hot inner solar system, and consist entirely of nominally anhydrous minerals (Weisberg and Kimura, 2012). As such, Earth's building blocks have long been presumed to have been 'dry', and so provided negligible water to the proto-Earth (e.g., Marty, 2012; Morbidelli et al., 2000). This concept has recently been reinforced by measurements of very low water concentrations in nominally anhydrous silicates in aubrites (achondrites isotopically resembling ECs) (Peterson et al., 2023). Although it is unclear what proportion of hydrogen (and other volatile elements) would survive processes such as planetary degassing and differentiation, these measurements could imply that enstatite chondrites were effectively devoid of water.

Several processes have been suggested to have then provided water to our planet later in its history. These include a late veneer of hydrated cometary material (Owen and Bar-Nun, 1995), and delivery via bombardment from outer-solar-system derived carbonaceous chondrite-like material (Alexander et al., 2012). These models imply that our planet's water budget – and by extension, its suitability for life – is the result of the stochastic scattering of outer solar system material into the terrestrial planet forming region (Morbidelli et al., 2000). In this case, habitability would not be a natural consequence of Earth's formation from EC-like material.

Contrarily, recent measurements of the bulk compositions of ECs reveal they may unexpectedly contain high hydrogen concentrations (0.08–0.54 wt% H_2O)(Piani et al., 2020; Thomassin et al., 2023). Indeed, these measurements suggest ECs seemingly carry enough of this ingredient of water to account for up to ~14 times the mass of Earth's oceans. Moreover, isotopic measurements argue that Earth may have

* Corresponding author.
E-mail address: thomas.barrett@st-annes.ox.ac.uk (T.J. Barrett).

https://doi.org/10.1016/j.icarus.2025.116588
Received 27 November 2024; Received in revised form 24 March 2025; Accepted 31 March 2025
Available online 3 April 2025

accreted as much as ~70 % of its volatile inventory, including hydrogen and nitrogen, from inner solar system material (Martins et al., 2023; Piani et al., 2020; Savage et al., 2022; Steller et al., 2022). Later delivery of outer solar system material then likely contributed small amounts of volatile elements, which help to resolve the observed hydrogen and nitrogen isotopic ratios of Earth's surface (Alexander et al., 2012; Piani et al., 2020). Combined, these findings suggest that Earth, and other terrestrial planets, may have in fact formed with high initial inventories of hydrogen and other volatiles. However, one pivotal unknown in these recent measurements is the phase that carries ~80 % of the bulk hydrogen concentration in ECs. Without this information, our understanding of the reason this element may be present in these meteorites in such high concentrations is severely limited.

In all, current observations disagree on the hydrogen content of ECs. As such, it is unclear whether the proto-Earth contained abundant hydrogen from its inception or whether this element was predominantly delivered to our planet after the main stage of its formation. It is therefore currently unknown whether Earth's water is a natural outcome of its formation from EC-like material. To explore the amount of native hydrogen in ECs as well as examine the phase that may host this element in these meteorites, here we map an EC using micrometre-scale X-ray absorption near edge structure spectroscopy at the sulfur K edge (S-XANES).

2. Materials and methods

We explored the speciation of S, and the abundance of different species of this element, in the EH3 chondrite LAR 12252 using micrometre-scale S-XANES at beamline I18 at the Diamond Light Source. We chose to study LAR 12252 due to its low weathering grade of A and a description of only modest terrestrial alteration. This low amount of weathering minimises the likelihood of widespread and/or prevalent terrestrial H-bearing weathering products.

We measured a 2D S-XANES map of an area of clastic matrix in this meteorite. This region included fragments of chondrules (which included mesostasis), enstatite grains, metal grains, various sulfide grains, and fine matrix (composed of an assortment of materials, all <5 μm). We measured these maps by sweeping an X-ray beam with a 5 μm spot size in 5 μm steps over an area 470 × 480 μm^2 large and measuring an S-XANES spectrum at each step (resulting in a total of 9024 spectra). The energy of the beam was increased from 2465 to 2495 eV in 0.2 eV intervals at each individual spot, with an acquisition time of 0.05 s at each energy value. The mapped area was selected to minimise the number of large objects (≳100 μm) and visible signs of terrestrial weathering, such as rust. We also measured 15 spot spectra at points within mesostasis in 6 chondrules throughout our thin section, as well as in multiple cracks containing terrestrial weathering products. Chondrule mesostasis spots were selected following optical microscopy, ensuring that they represented the range of chondrule sizes and types present in the thin section.

To analyse our data, we fitted all our S-XANES spectra with multiple Gaussian curves using IGOR Pro, discussed further in the SI. We chose this method over linear combination fitting due to the heterogeneities within the sample, absence of a complete reference database of spectra collected from meteorites, and the number of spectra collected. We initially fitted each spectrum only between 2465 and 2478 eV (Fig. 1b) because this energy range contains the iron sulfide peak, the H—S peak, and parts of the S-edge step function and peaks due to S species at higher energies. We chose this approach because it allowed us to focus on the peaks of interest, making the fitting procedure more robust and straightforward (see SI). As seen in Fig. 1, this method produced only small fitting errors (discussed further in the SI). To determine the amplitude of the S^{6+} peak, we then fitted a single Gaussian curve in the energy range 2580–2590 eV. This approach means the recovered height of this peak is that above the background in this energy range, so it isolates the S^{6+} signal by not considering the S-edge step function or any other S species. To explore the amount of H—S throughout our mapped area of LAR 12252, we calculated the enrichment/depletion of H—S at each point in mapped area by normalising the amplitude of the H—S peak recovered from each spectrum to the average amplitude of this peak recovered from the 15 spot spectra of chondrule mesostasis. Chondrule mesostasis contains a heterogenous H concentration with a

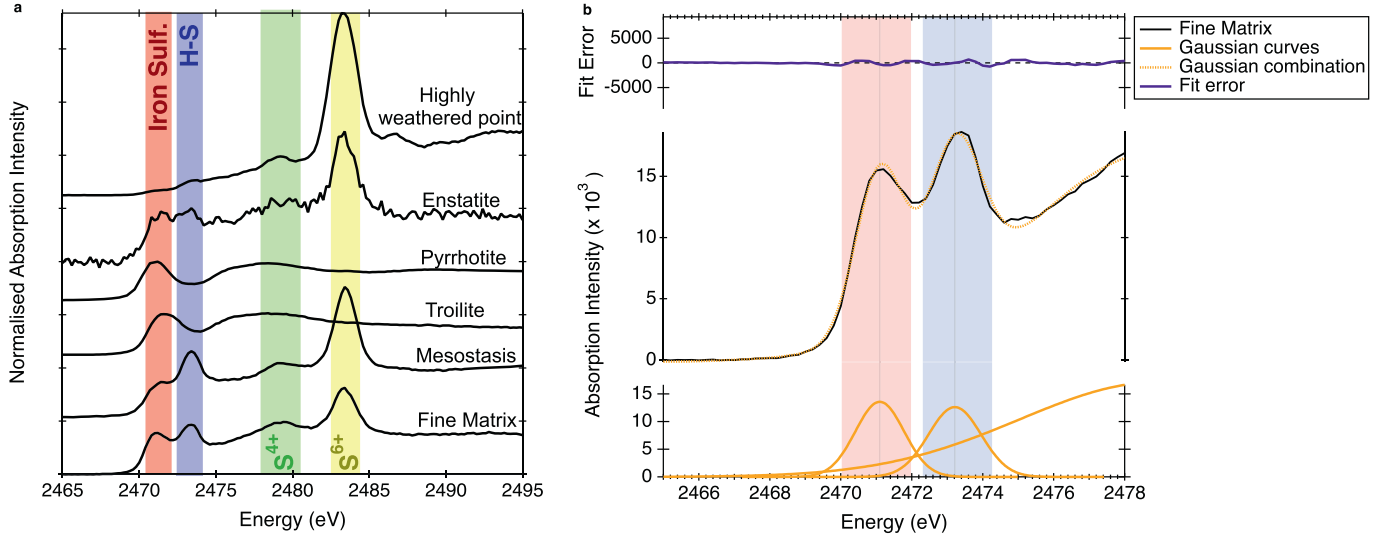

Fig. 1. a. Representative S-XANES spectra measured in a variety of different phases in LAR 12252 during this study. Positions of peaks ascribed to species from reference spectra *(e.g., Anzures et al., 2019; Lerner et al., 2021; Prange et al., 2002)* are highlighted by vertical coloured bars. Spectra are normalised, so amplitudes here do not reflect sulfur content. Spectra from enstatite grains appear noisy due to very low sulfur counts, and closely resemble spectra measured in metal grains. The sulfur signal in these non-sulfur bearing phases are likely caused by minor sampling of matrix that could be adjacent to, or underneath these phases, or the presence of small amounts of sulfur-bearing impurities within these phases. 1b Peak fitting method used to extract the amplitudes of the iron sulfide and H—S peaks from the fine matrix spectra in 1a. We achieved this multi-peak approach by creating a total fit (dashed orange in middle panel) from three Gaussian curves (orange, bottom panel) across the energy range 2468–2478 eV. This process yields small residual errors (purple, top panel). The dashed line in the top panel marks zero, and the total variation in the scale is set as the same as that in the central panel. The highlighted peaks correspond to the same as in Fig. 1a. (For interpretation of the references to colour in this figure legend, the reader is referred to the web version of this article.)

fairly wide range of measured values (Piani et al., 2020; Thomassin et al., 2023). This natural spread in concentration reflected itself in our study as a wide range of H—S peak amplitudes in mesostasis, which introduced the largest source of error in this study (discussed further in the SI). We isolated spectra that correspond to fine matrix using peak amplitude ratios (discussed further in the SI).

3. Results

3.1. Peak identification

The S-XANES spectra we collected display a variety of peaks, the presence of which depends principally on the phase that was measured (Fig. 1a). S-XANES spectra of fine matrix and mesostasis typically contain four peaks (Fig. 1a), providing evidence of sulfur in different compounds and oxidation states in these phases. By comparing peak energy and shape to reference spectra (e.g., Anzures et al., 2019; Lerner et al., 2021; Prange et al., 2002)$^{-}$as well as from the Database of Inorganic Sulfur Compounds from The European Synchrotron Radiation Facility, we can identify the species responsible for each peak.

The peak at lowest energy, highlighted in red in Fig. 1, is widespread in fine matrix and mesostasis and is ascribed to submicron iron sulfides (troilite and pyrrhotite) (Anzures et al., 2019; Fleet, 2005; Klimm et al., 2012; Métrich et al., 2009). The energy of this peak varies from 2471.8 eV to 2471.2 eV, diagnostic of the composition of this mineral shifting from stoichiometric troilite to pyrrhotite ($Fe_{1-x}S$, $0 < x < 0.125$) (Head et al., 2018). Energies of all peaks detected in our spectra are slightly (~1 eV) higher than reported in most previous studies (e.g., Anzures et al., 2019; Fleet, 2005; Klimm et al., 2012; Métrich et al., 2009), but remained constant throughout the duration of our study. Such variations are common across XANES studies and are attributed to differences in calibration of the monochromator (see SI).

Throughout the fine matrix and mesostasis, we also find a distinctive peak at ~2473.2 eV, highlighted in blue in Fig. 1. Due to similar peak locations in reference spectra, this peak could be due to hydrogen bonded to S, native S, or pyrite (Bose et al., 2024). However, based on previously reported spectra of H_2S trapped in silicate glasses, gaseous H_2S, and thiol groups (Bodeur and Esteva, 1985; Bose et al., 2024; Klimm et al., 2012; Orthous-Daunay et al., 2010; Prange et al., 2002), the peak location relative to those of FeS and S^{6+}, and the absence of elemental S in previous sub-micron-scale compositional measurements (Lehner et al., 2014), we ascribe this peak to S bonded to H. Additionally, if this peak was caused by elemental S, rather than H—S, we would expect a broadening/shifting to higher energy of the wide absorption peak highlighted in green in Fig. 1 than we observe. Our observation of H—S in chondrule mesostasis supports previous Raman spectroscopy measurements of the H—S bond in this phase (Thomassin et al., 2023). Additionally, our finding of the H—S peak throughout fine matrix demonstrates that H—S is a common form of hydrogen in ECs, and that this form of hydrogen is present in multiple phases.

In addition to reduced sulphides, many spectra also contain a peak at ~2483.4 eV corresponding to S^{6+}, the most oxidised form of sulfur, highlighted in yellow in Fig. 1. The amplitudes of these peaks vary widely among the points we measured, and they are at their highest in spot spectra collected within cracks where clear terrestrial weathering has occurred (Fig. S3). They also exist at much lower, but still variable, amplitudes in matrix and mesostasis. Different sulfates can be difficult to distinguish using S-XANES because different cations do not cause large shifts in peak energy (Anzures et al., 2019). Despite this, we were able to identify $CaSO_4$ and $FeSO_4$ at some points in our mapped area of matrix, owing to minor peaks in the pre- and post-edge regions of the spectra (Anzures et al., 2019). The S^{6+} peak is absent within macroscopic (>10 μm) grains of metal, enstatite, and sulfides.

Finally, we observe a small peak centred on ~2478 eV, shown in green in fig. 1. The amplitude of this peak is affected by two species: a second, wide absorption feature of troilite and pyrrhotite; and small amounts of S^{4+} likely formed through gradual photo-reduction of S^{6+} by the X-ray beam (Lerner et al., 2021; Wilke et al., 2008). We minimised the impact of photoreduction by mapping with as short acquisition times as possible.

3.2. Hydrogen abundance

Because peak amplitude correlates with species abundance (Anzures et al., 2019; Fleet, 2005; Klimm et al., 2012), we are able to explore concentrations of the different species in the matrix of LAR 12252 using S-XANES spectra. However, the nature of complex geological samples like meteorites (e.g., the wide range of measured H concentrations in mesostasis) introduces specific challenges that make absolute concentrations difficult to determine reliably via comparisons to datasets collected using other techniques (e.g., Piani et al., 2020; Thomassin et al., 2023). However, we were able to estimate the relative concentration of H—S in EC matrix by comparing the amplitude of the peak at ~2473.2 eV throughout our map to the average amplitude of this peak we measure in chondrule mesostasis. We found that our clastic matrix region contains points with H—S peak amplitudes that vary from 0 - ~40 times the average mesostasis amplitude (Fig. 2b). The lowest relative amplitudes are found within the interiors of macroscale enstatite, metal, and sulfide grains. The highest amplitudes are in regions of fine matrix. Excluding points with more extensive terrestrial weathering (in the form of large S^{6+} peaks, see *Discussion* section; Fig. S5), we calculate that fine matrix in LAR 12252 contains an average of 9.8 ± 3.1 times as much H—S as chondrule mesostasis in this meteorite (2 standard error, calculated from the measured mesostasis H—S peak amplitudes; discussed further in SI).

By combining this value with the proportion of fine matrix in EH3 chondrites, we are able to constrain the relative contribution of fine matrix towards the H budget of these meteorites. Unfortunately, the parameters used to calculate the proportion of fine matrix have not been measured for LAR 12252, so we chose to use parameters measured from the paired EH3 chondrites SAH 97072 and SAH 97096. We adopted this approach because these meteorites are particularly well-studied, their bulk and mesostasis H concentrations have been measured previously (Piani et al., 2020), and the proportion of fine matrix is likely similar among most EH3 chondrites (±2 vol%; Lehner et al., 2014). As such, the value we calculate is likely relevant to the enrichment factor we recovered from LAR 12252. Using grain (3730 kg m^{-3}) and bulk (3240 kg m^{-3}) densities (Macke et al., 2010), the volume fraction of clastic matrix (21.5 vol%; Lehner et al., 2014), and the proportion of fine matrix in clastic matrix (~50 vol%) in these meteorites (Rubin et al., 2009), we calculate a mass fraction of fine matrix (Bryson and Brennecka, 2021) of ~4.8 wt%. This value is approximately half that of chondrule mesostasis in the same meteorites (9.3 wt%; Piani et al., 2020). As such, assuming fine matrix in these meteorites also carries on average ~ 9.8 times as much H as mesostasis, fine matrix would contribute an average of ~5 times more H to the bulk H concentration than mesostasis.

Using this factor, we can explore whether this H—S enrichment in fine matrix corresponds to a significant amount of H. For reference, previous studies have found that mesostasis accounts for an average of ~13 % of the bulk H concentration in SAH 97096 (Piani et al., 2020). Because they have not been measured previously, it is unknown whether other EH3 chondrites share equally high mesostasis H concentrations. However, combining our recovered enrichment factor with this proportion of H in mesostasis argues that fine matrix likely contributes a significant amount of H towards the bulk concentration in EH3 chondrites (several tens of wt%), and could account for the majority of H in these meteorites.

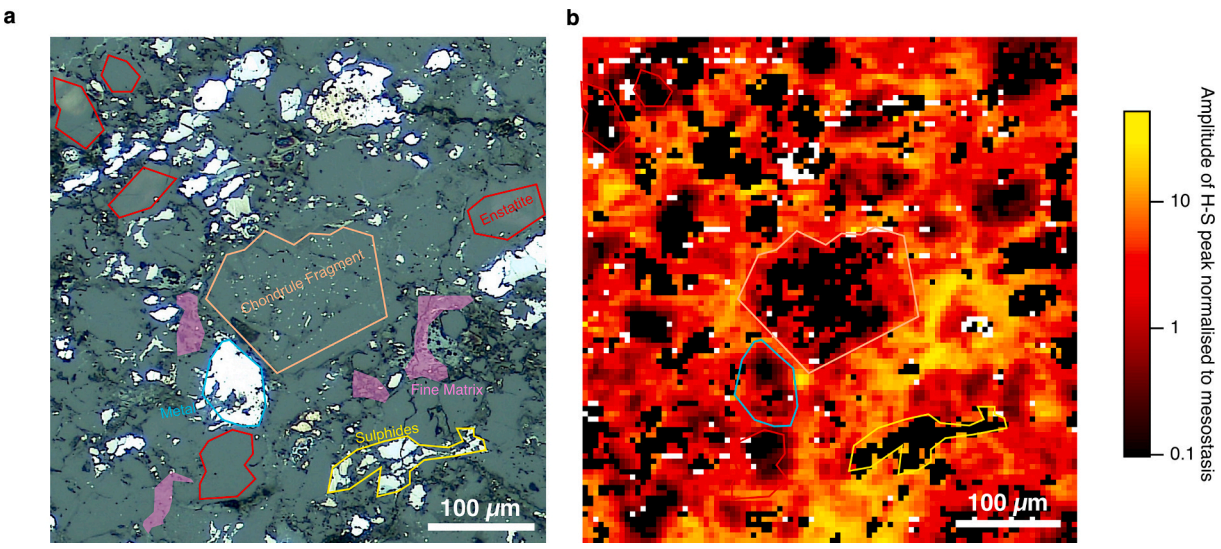

Fig. 2. a. Optical microscopy image of the clastic matrix region in LAR 12252 that was studied using S-XANES. Notable phases include enstatite (examples outlined in red), sulphides (example outlined in yellow), a small chondrule fragment (outlined in orange), and fine matrix (examples highlighted in pink). b Corresponding map calculated from the S-XANES spectra of the region shown in a, showing the amplitude of the H—S peak at each point normalised to the average amplitude of point spectra measured from chondrule mesostasis (Fig. S8). Black pixels correspond to points where the S-XANES spectra that did not contain a resolvable H—S peak. White pixels correspond to points where the S-XANES spectra could not be fitted due to their quality or noise in the spectra. Some grain outlines have been transferred onto Fig. 2b to allow for comparison of the two figures. (For interpretation of the references to colour in this figure legend, the reader is referred to the web version of this article.)

4. Discussion

4.1. Is EC hydrogen native or a product of terrestrial weathering?

The primary difficulty with measuring the hydrogen content of a meteorite is ensuring that the hydrogen is not a product of terrestrial weathering. This is especially pertinent in ECs, where rare sulphide phases such as oldhamite react readily with atmospheric moisture to produce hydrated sulfates (Avril et al., 2021; Bland et al., 2006; Okada et al., 1981). While we avoided areas with extensive visible terrestrial weathering products, such as rust, much of the remaining meteorite could still have been modified by terrestrial weathering. Indeed, it has been suggested that previous measurements of bulk EC hydrogen concentrations were substantially influenced by the presence of terrestrial water/OH^- contained in weathering products (Peterson et al., 2023).

Fig. 1 shows a peak at 2483.4 eV, attributed to the presence of oxidised, S^{6+}-bearing species. However, the pre-terrestrial minerals observed petrographically in pristine ECs (including niningerite, oldhamite, and Si-bearing metal) argue these meteorites formed under particularly reducing conditions (Weisberg and Kimura, 2012) that will have led to the total absence of S^{6+}-bearing minerals (Klimm et al., 2012). As such, the presence of S^{6+}-bearing phases is most easily explained by terrestrial weathering, most likely of native sulfides. This is reinforced by spot spectra measured from a rust-bearing crack in the meteorite, which contained the highest S^{6+} peak amplitudes we measured (Fig. S3). Additionally, a grain of native troilite that has another crack running through it has been transformed into pyrrhotite via reactions with terrestrial water (Fig. S4). Crucially, these two crack spectra contain either no resolvable H—S peak at ~2473.2 eV (the crack containing terrestrial pyrrhotite; Fig. S4) or one of very small amplitude relative to the S^{6+} peak (Fig. S3). Together, these observations suggest that H—S is not a weathering product, so is instead native to EH3 meteorites.

Nonetheless, we chose to still filter the points we analysed to include only those that experienced the lowest extents of terrestrial weathering. We monitored this extent of weathering in each spectrum primarily using the ratio of the amplitude of the S^{6+} peak to that of the FeS peak; as terrestrial weathering converted sulfide to sulfate (Bland et al., 2006) this ratio will have increased (Fig. S5). This ratio varied widely throughout our mapped area, demonstrating that the local extent of terrestrial weathering was strongly heterogenous and was very low in some places (Fig. S6). To minimise the impact of weathering, we chose to only include spectra with an S^{6+}:FeS peak amplitude ratio < 0.5 in our analysis (Fig. S5), which we consider to be the most pristine (see SI).

4.2. Abundance of H

Our analysis demonstrates that native H—S exists in fine matrix and mesostasis in ECs, and is in highest concentrations in fine matrix. These observations support previous studies that observed a relationship between S and H concentrations in mesostasis as well as the S—H bond in this phase using Raman spectroscopy (Thomassin et al., 2023). As such, S—H appears to be widespread in ECs.

Our S-XANES analysis suggests that fine matrix accounts for an average of ~5 times as much H—S as mesostasis in LAR 12252. This finding argues that fine matrix is likely the dominant source of H in EH3 chondrites and H—S is likely the dominant form of H in these meteorites. Combined with the observation of the S—H bond in mesostasis alongside previous measurements of the amount of H in organic matter in ECs (Piani et al., 2012), our observation of significant quantities of H in fine matrix mean it is likely that ECs carried more H than had been previously considered based on their petrology (e.g. Marty, 2012). This finding supports recent studies that find relatively high bulk H concentrations in EH3 chondrites (Piani et al., 2020). In all, EH3 chondrites appear to contain higher concentrations of native H, in the form of H—S, than previously thought, which is possibly capable of explaining the entire water budget of the present-day Earth (Piani et al., 2020).

4.3. Source of H

Despite appearing to host significant amounts of hydrogen in ECs, the phase that carries the H—S bond we identified, and how it formed, were previously unknown. Investigating this further, we found that spectra with large H—S peak amplitudes also exhibited large Fe—S peak amplitudes. In fact, the ratio of these two peak amplitudes varies between only ~0–1 (Fig. 3) despite absolute amplitudes of these peaks,

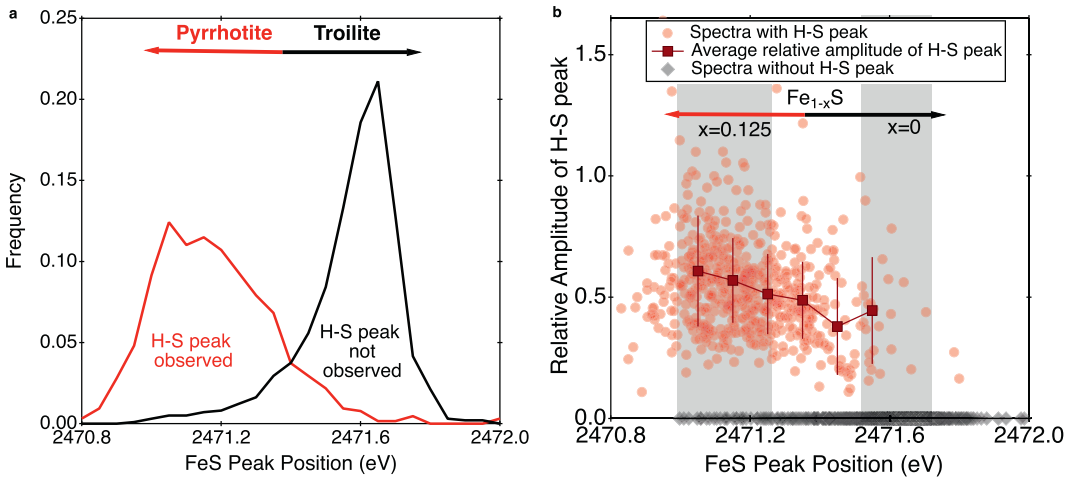

Fig. 3. a. The distribution of the position of the FeS peak in all points throughout the mapped area for spectra with (red) and without (black) resolvable H—S peaks. Spectra with energies of the iron sulfide peak that indicate pyrrhotite is the dominant sulfide are more likely to carry the H—S peak, while spectra with iron sulfide peak energies consistent with troilite are less likely to display an H—S peak. b The amplitude of the H—S peak normalised to the amplitude of the corresponding FeS peak from each spectrum, plotted against the peak position of the FeS peak, from points included in final analysis. Grey bars indicate the peak location of endmember troilite and pyrrhotite. The transition between these bars represents a change in x in the pyrrhotite chemical formula, $Fe_{1-x}S$, $0 < x < 0.125$. Black diamonds on the horizontal axis represent spectra with no resolvable H—S peak. The dark red squares represent averages of the individual points in 0.1 eV-wide bands. The relative amplitude of the H—S peak increases as the abundance of pyrrhotite increases, suggesting pyrrhotite is linked to hydrogen in ECs. The slight increase at higher energy reflects the low number of points in this energy region containing an H—S peak, and difficulties identifying the H—S peak when its amplitude is small. (For interpretation of the references to colour in this figure legend, the reader is referred to the web version of this article.)

and relative amplitudes between other pairs of peaks, varying by several orders of magnitude throughout our mapped area (Fig. S2). This relationship suggests that the concentration of H—S is linked to the abundance of iron sulfides.

This variation in relative peak amplitudes can be used to further explore the origin of hydrogen in ECs. We found that spectra with a resolvable H—S peak (i.e., ratio of H—S peak amplitude to iron sulfide peak amplitude >0) tend to contain an iron sulfide peak at lower energies than those that do not contain a resolvable H—S peak (Fig. 3a). The energy of the iron sulfide peak reflects the stoichiometry of this phase, with the peak shifting the lower energy as the mineral become more iron deficient (i.e., as the mineralogy evolves from troilite to pyrrhotite; Head et al., 2018; fig. S4). This observation suggests that hydrogen is associated with pyrrhotite in ECs.

We can explore this in more detail by examining the relative peak amplitude of each individual spectrum. We find a trend between the energy position of each sulfide peak and the relative peak amplitude of the H—S peak (Figs. 3b, S1). This relationship further indicates that the abundance of the H—S bond increases gradually as the amount of pyrrhotite increases. Together, these observations argue that pyrrhotite is key to the source of H.

The presence of pyrrhotite is perhaps unexpected given the very reducing nebular environment in which ECs formed (Schrader et al., 2021; Weisberg and Kimura, 2012). Previous measurements of the concentrations of iron sulfides in ECs made using electron probe microanalysis find near-stoichiometric compositions in iron sulfides (Piani et al., 2016; Schrader et al., 2021). Our S-XANES spectra support this result, with the spectra from the centre of macroscopic (≳10 μm) iron sulfides in our map matching reference spectra of troilite (Fig. 1a). However, in the fine matrix and approaching the edges of some macroscopic sulfide grains, the energy of the Fe—S peak shifts to lower values (Fig. S7). This shift argues that pyrrhotite exists as micron- to sub-micron-scale grains in fine matrix and micron- to sub-micron-scale rims on larger troilite grains. Although nebular troilite is more common, nebular pyrrhotite has been observed previously in multiple submicron settings: as rims ~50 nm wide coating larger grains of troilite in carbonaceous chondrites (Harries and Langenhorst, 2013); in the matrix of ECs as submicron grains (Lehner et al., 2014); and as <50 nm grains in anhydrous interplanetary dust particles (Zolensky and Thomas, 1995). Combined with our results, these observations argue that iron sulphides exist as pyrrhotite when they are submicron in scale. This pyrrhotite has been proposed to have formed through low temperature sulfidation of pre-existing troilite in a high fS_2 environment in the disk (Harries and Langenhorst, 2013; Kerridge, 1976; Zolensky and Thomas, 1995), or alternatively through the sulfidation of Fe metal by H_2S (Gainsforth et al., 2017). Our results suggest this former process occurred only on the outer part (perhaps <1 μm) of troilite grains, which would cause an entire troilite grain to transform to pyrrhotite if it was below this critical size.

While our analysis indicates that points containing more submicron pyrrhotite are also rich in H—S, the coarse X-ray spot size (5 μm) means we cannot observe whether submicron pyrrhotite itself is the carrier phase. If pyrrhotite were the carrier of this hydrogen, we might expect $Fe_7S_8H_2$ to be present, where iron vacancies are filled by two hydrogen atoms (Cabedo et al., 2024). This phase would be 0.31 wt% H, which would correspond to lower enrichment factors than we measure in points in the fine matrix (Fig. 2b). This difference argues that hydrogen sequestered directly in the structure of pyrrhotite cannot alone explain the concentrations of H—S measured in fine matrix, and another H bearing phase must be present.

Pyrrhotite in ECs is often enclosed in amorphous SiO_2-rich material (Lehner et al., 2014), a phase known to store hydrogen bonded to sulfur in these meteorites (Thomassin et al., 2023). Such glassy material could have formed if grains of pyrrhotite accumulated dust particles when they were free-floating in the disk and these assemblages experienced flash heating events. As demonstrated by Cabedo et al. (2024), the elevated temperatures during these events would have led to H_2S being produced through the sacrificial catalytic reaction of pyrrhotite with nebular H_2. Due to their adjoining nature, this H_2S could have dissolved into the molten silicate, where it would become trapped upon glass formation during rapid cooling. As such, we propose that H is trapped in the form of H_2S in glassy silicate material that encases grains of pyrrhotite (Lehner et al., 2014). This would mean that the peak we measure in our S-XANES spectra is due to H_2S trapped in silicate glass, as has been observed previously (e.g., Klimm et al., 2012). This process can be summarised through the following reactions, and Fig. 4:

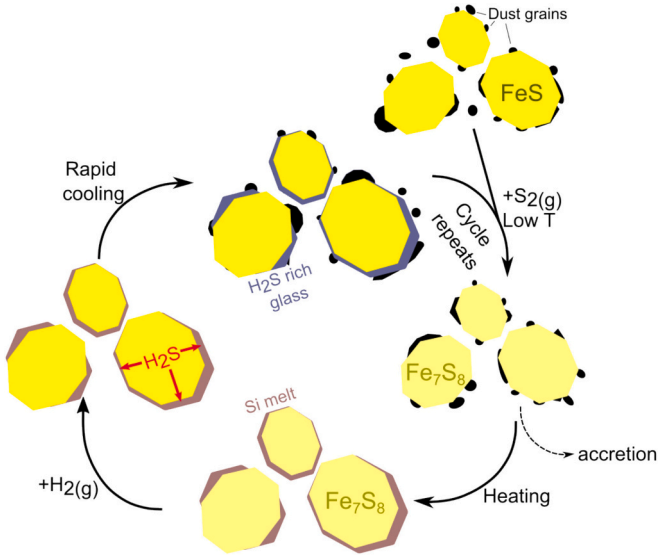

Fig. 4. Schematic outlining the process through which H could be sequestered into ECs. Firstly, submicron FeS grains that become coated in dust particles in the solar nebula are transformed into pyrrhotite at low temperatures in a high fS_2 environment (e.g. Zolensky and Thomas, 1995). Next, during flash heating events, a sacrificial catalysis reaction with H_2 at produces H_2S (Cabedo et al., 2024), which is trapped in silicate melt that sits around the grains of sulphide formed when the dust grains melt. Finally, this assembles rapidly cools, produce sulfide grains that are coated in silicate glass, which hosts trapped H_2S. This process can repeat, with further dust accumulating onto the surface of the Si-rich glass after it first forms. During/following low temperature sulfidation, accretion can occur to form planetesimals. This cycle results in pyrrhotite existing on a sub-micron length scale surrounded by H—S bearing silicate glassy material, consistent with our S-XANES measurements.

$$7FeS + \frac{1}{2}\,S_{2(g)} \underset{low\ T}{\rightarrow} Fe_7S_8 \quad (1)$$

$$Fe_7S_8 + H_{2(g)} \underset{high\ T}{\rightarrow} 7FeS + H_2S \quad (2)$$

Our data also indicate that hydrogen in chondrule mesostasis and fine matrix are stored in similar ways: predominantly within SiO_2-rich glass either contain or are associated with sub-micron sulfide grains. In this case, the carrier phase is the same across both mesostasis and matrix, and we therefore chose not to apply a correction for the phase that carries hydrogen when calculating relative hydrogen peak amplitudes in the matrix compared to mesostasis.

4.4. Implications

In conventional models of the origin of volatile elements on Earth, water was the result of a stochastic, late bombardment of carbonaceous material onto our planet (Alexander et al., 2012). This scenario is capable of explaining Earth's water budget, but means that water and habitable conditions on Earth are a result of a chance scenario. The combined D and ^{15}N compositions of the oceans and atmosphere compared to the mantle (Piani et al., 2020) indicate that there is a contribution from this carbonaceous source, at least on the surface of our planet. However, the D and ^{15}N isotopic composition of the mantle have been used to argue that this bombardment struggles to explain the bulk of the hydrogen within our planet (Piani et al., 2020). As such, volatiles delivered by bombardment likely correspond to a small proportion of the total budget throughout Earth.

Our findings suggest that H—S in fine matrix in EH3 chondrites is native and potentially the dominant source of H in these meteorites, and that this phase may account for the majority of their bulk H concentrations. These findings indicate that pristine ECs could contain enough hydrogen to explain the entire water budget of our planet, requiring that less water needs to have been delivered to Earth after the main stage of its formation. In this scenario, ECs seemingly became enriched in hydrogen through sulfidation of submicron troilite in an S_2-rich nebular gas to form pyrrhotite, which then catalysed a reaction producing H_2S that became trapped in adjoining silicate-rich glass. As such, the water budget of Earth does not need to be the result of a chance bombardment. Instead, it can be a natural and determined consequence of the formation of EC-like material in the hot, reducing, and sulfidising environment of the inner solar system. Additionally, this means that other terrestrial planets that have been proposed to have formed from similar material and in similar environments – including Mars (Brasser et al., 2018), Mercury (Namur et al., 2016), and perhaps Venus – could have had similar early volatile budgets to the proto-Earth as a result of their primary feedstock. A key question now is the hydrogen content of metamorphosed ECs (e.g., EH4-EH6) and aubrites, as well as the proportions of each of these types of meteorites in the proto-Earth.

CRediT authorship contribution statement

Thomas J. Barrett: Writing – review & editing, Writing – original draft, Investigation, Conceptualization. **James F.J. Bryson:** Writing – review & editing, Supervision, Investigation. **Kalotina Geraki:** Writing – review & editing, Investigation.

Declaration of competing interest

The authors declare that they have no known competing financial interests or personal relationships that could have appeared to influence the work reported in this paper.

Acknowledgements

The authors would like to thank Diamond Light Source for beamtimes (proposals SP31591-1 and SP35606), and staff of beamline I18 for assistance with data collection. The authors would also like to thank the Antarctic Search for Meteorites (ANSMET) program (which has been funded by NSF and NASA and curated by the Department of Mineral Sciences of the Smithsonian Institution and Astromaterials Curation Office at NASA Johnson Space Center) for use of their meteorite samples. JFJB acknowledges funding through UKRI grant number EP/Y014375/1. TJB acknowledges funding through STFC.

Data availability

Data is available on a Zenodo repository, found at the following address. https://doi.org/10.5281/zenodo.12156050.

References

Alexander, C.M.O'D., Bowden, R., Fogel, M.L., Howard, K.T., Herd, C.D.K., Nittler, L.R., 2012. The provenances of asteroids, and their contributions to the volatile inventories of the terrestrial planets. Science 337 (6095), 721–723. https://doi.org/10.1126/science.1223474.

Anzures, B., Parman, S., Milliken, R., Lanzirotti, A., Newville, M., 2019. XANES spectroscopy of sulfides stable under reducing conditions. Am. Mineral. https://doi.org/10.2138/am-2020-7146.

Avril, C., Malavergne, V., van Hullebusch, E.D., Brunet, F., Borensztajn, S., Labanowski, J., Hennet, L., Guyot, F., 2021. Aqueous alteration and bioalteration of a synthetic enstatite chondrite. Meteorit. Planet. Sci. 56 (3), 601–618. https://doi.org/10.1111/maps.13641.

Bland, P.A., Zolensky, M.E., Benedix, G.K., Sephton, M.A., 2006. *Weathering of chondritic meteorites* (p. 853). https://ui.adsabs.harvard.edu/abs/2006mess.book..853B.

Bodeur, S., Esteva, J.M., 1985. Photoabsorption spectra of H2S, CH3SH and SO2 near the sulfur K edge. Chem. Phys. 100 (3), 415–427. https://doi.org/10.1016/0301-0104(85)87067-1.

Bose, M., Root, R.A., Guan, Y., Eaton, J., Wittmann, A., Skrmetti, T., Desch, S.J., 2024. Evidence of both molecular cloud and fluid chemistry in Ryugu regolith. Sci. Adv. 10 (30), eadp3037. https://doi.org/10.1126/sciadv.adp3037.

Brasser, R., Dauphas, N., Mojzsis, S.J., 2018. Jupiter's influence on the building blocks of Mars and earth. Geophys. Res. Lett. 45 (12), 5908–5917. https://doi.org/10.1029/2018GL078011.

Bryson, J.F.J., Brennecka, G.A., 2021. Constraints on Chondrule generation, disk dynamics, and asteroid accretion from the compositions of carbonaceous meteorites. Astrophys. J. 912 (2), 163. https://doi.org/10.3847/1538-4357/abea12.

Cabedo, V., Pareras, G., Allitt, J., Rimola, A., Llorca, J., Yiu, H.H.P., McCoustra, M.R.S., 2024. Reactivity of chondritic meteorites under H2-rich atmospheres: formation of H2S. Mon. Not. R. Astron. Soc. 2520. https://doi.org/10.1093/mnras/stae2520.

Dauphas, N., 2017. The isotopic nature of the earth's accreting material through time. Nature 541 (7638), 521–524. https://doi.org/10.1038/nature20830.

Fleet, M.E., 2005. Xanes spectroscopy of sulfur in earth materials. Can. Mineral. 43 (6), 1811–1838. https://doi.org/10.2113/gscanmin.43.6.1811.

Gainsforth, Z., Lauretta, D.S., Tamura, N., Westphal, A.J., Jilly-Rehak, C.E., Butterworth, A.L., 2017. Insights into solar nebula formation of pyrrhotite from nanoscale disequilibrium phases produced by H2S sulfidation of Fe metal. Am. Mineral. 102 (9), 1881–1893. https://doi.org/10.2138/am-2017-5848.

Harries, D., Langenhorst, F., 2013. The nanoscale mineralogy of Fe,Ni sulfides in pristine and metamorphosed CM and CM/CI-like chondrites: tapping a petrogenetic record. Meteorit. Planet. Sci. 48 (5), 879–903. https://doi.org/10.1111/maps.12089.

Head, E., Lanzirotti, A., Newville, M., Sutton, S., 2018. Vanadium, sulfur, and iron valences in melt inclusions as a window into magmatic processes: a case study at Nyamuragira volcano, Africa. Geochim. Cosmochim. Acta 226, 149–173. https://doi.org/10.1016/j.gca.2018.01.033.

Javoy, M., Kaminski, E., Guyot, F., Andrault, D., Sanloup, C., Moreira, M., Labrosse, S., Jambon, A., Agrinier, P., Davaille, A., Jaupart, C., 2010. The chemical composition of the earth: enstatite chondrite models. Earth Planet. Sci. Lett. 293 (3), 259–268. https://doi.org/10.1016/j.epsl.2010.02.033.

Kerridge, J.F., 1976. Formation of iron sulphide in solar nebula. Nature 259 (5540), 5540. https://doi.org/10.1038/259189a0.

Klimm, K., Kohn, S.C., Botcharnikov, R.E., 2012. The dissolution mechanism of Sulphur in hydrous silicate melts. II: solubility and speciation of Sulphur in hydrous silicate melts as a function of fO2. Chem. Geol. 322–323, 250–267. https://doi.org/10.1016/j.chemgeo.2012.04.028.

Lehner, S.W., McDonough, W.F., Németh, P., 2014. EH3 matrix mineralogy with major and trace element composition compared to chondrules. Meteorit. Planet. Sci. 49 (12), 2219–2240. https://doi.org/10.1111/maps.12391.

Lerner, A.H., Muth, M.J., Wallace, P.J., Lanzirotti, A., Newville, M., Gaetani, G.A., Chowdhury, P., Dasgupta, R., 2021. Improving the reliability of Fe- and S-XANES measurements in silicate glasses: correcting beam damage and identifying Fe-oxide nanolites in hydrous and anhydrous melt inclusions. Chem. Geol. 586, 120610. https://doi.org/10.1016/j.chemgeo.2021.120610.

Macke, R.J., Consolmagno, G.J., Britt, D.T., Hutson, M.L., 2010. Enstatite chondrite density, magnetic susceptibility, and porosity. Meteorit. Planet. Sci. 45 (9), 1513–1526. https://doi.org/10.1111/j.1945-5100.2010.01129.x.

Martins, R., Kuthning, S., Coles, B.J., Kreissig, K., Rehkämper, M., 2023. Nucleosynthetic isotope anomalies of zinc in meteorites constrain the origin of Earth's volatiles. Science (New York, N.Y.) 379 (6630), 369–372. https://doi.org/10.1126/science.abn1021.

Marty, B., 2012. The origins and concentrations of water, carbon, nitrogen and noble gases on earth. Earth Planet. Sci. Lett. 313–314, 56–66. https://doi.org/10.1016/j.epsl.2011.10.040.

Métrich, N., Berry, A.J., O'Neill, H.St., C., & Susini, J., 2009. The oxidation state of sulfur in synthetic and natural glasses determined by X-ray absorption spectroscopy. Geochim. Cosmochim. Acta 73 (8), 2382–2399. https://doi.org/10.1016/j.gca.2009.01.025.

Morbidelli, A., Chambers, J., Lunine, J.I., Petit, J.M., Robert, F., Valsecchi, G.B., Cyr, K.E., 2000. Source regions and timescales for the delivery of water to the earth. Meteorit. Planet. Sci. 35 (6), 1309–1320. https://doi.org/10.1111/j.1945-5100.2000.tb01518.x.

Namur, O., Collinet, M., Charlier, B., Grove, T.L., Holtz, F., McCammon, C., 2016. Melting processes and mantle sources of lavas on mercury. Earth Planet. Sci. Lett. 439, 117–128. https://doi.org/10.1016/j.epsl.2016.01.030.

Okada, A., Keil, K., Taylor, G.J., 1981. Unusual weathering products of Oldhamite parentage in the Norton County enstatite Achondrite. Meteoritics 16 (2), 141–152. https://doi.org/10.1111/j.1945-5100.1981.tb00539.x.

Orthous-Daunay, F.-R., Quirico, E., Lemelle, L., Beck, P., deAndrade, V., Simionovici, A., Derenne, S., 2010. Speciation of sulfur in the insoluble organic matter from carbonaceous chondrites by XANES spectroscopy. Earth Planet. Sci. Lett. 300 (3), 321–328. https://doi.org/10.1016/j.epsl.2010.10.012.

Owen, T., Bar-Nun, A., 1995. Comets, impacts, and atmospheres. Icarus 116 (2), 215–226. https://doi.org/10.1006/icar.1995.1122.

Peterson, L.D., Newcombe, M.E., Alexander, C.M.O., Wang, J., Klein, F., Bekaert, D.V., Nielsen, S.G., 2023. The H content of aubrites: an evaluation of bulk versus in situ methods for quantifying water in meteorites. Earth Planet. Sci. Lett. 620, 118341. https://doi.org/10.1016/j.epsl.2023.118341.

Piani, L., Robert, F., Beyssac, O., Binet, L., Bourot-Denise, M., Derenne, S., Guillou, C.L., Marrocchi, Y., Mostefaoui, S., Rouzaud, J.-N., Thomen, A., 2012. Structure, composition, and location of organic matter in the enstatite chondrite Sahara 97096 (EH3). Meteorit. Planet. Sci. 47 (1), 8–29. https://doi.org/10.1111/j.1945-5100.2011.01306.x.

Piani, L., Marrocchi, Y., Libourel, G., Tissandier, L., 2016. Magmatic sulfides in the porphyritic chondrules of EH enstatite chondrites. Geochim. Cosmochim. Acta 195, 84–99. https://doi.org/10.1016/j.gca.2016.09.010.

Piani, L., Marrocchi, Y., Rigaudier, T., Vacher, L., Thomassin, D., Marty, B., 2020. Earth's water may have been inherited from material similar to enstatite chondrite meteorites. Science 369 (6507), 1110–1113. https://doi.org/10.1126/science.aba1948.

Prange, A., Dahl, C., Trüper, H.G., Behnke, M., Hahn, J., Modrow, H., Hormes, J., 2002. Investigation of S-H bonds in biologically important compounds by sulfur K-edge X-ray absorption spectroscopy. Eur. Phys. J. D - Atom. Mol. Optic. Plasma Phys. 20 (3), 589–596. https://doi.org/10.1140/epjd/e2002-00156-5.

Rubin, A.E., Griset, C.D., Choi, B.-G., Wasson, J.T., 2009. Clastic matrix in EH3 chondrites. Meteorit. Planet. Sci. 44 (4), 589–601. https://doi.org/10.1111/j.1945-5100.2009.tb00754.x.

Savage, P.S., Moynier, F., Boyet, M., 2022. Zinc isotope anomalies in primitive meteorites identify the outer solar system as an important source of earth's volatile inventory. Icarus 386, 115172. https://doi.org/10.1016/j.icarus.2022.115172.

Schrader, D.L., Davidson, J., McCoy, T.J., Zega, T.J., Russell, S.S., Domanik, K.J., King, A.J., 2021. The Fe/S ratio of pyrrhotite group sulfides in chondrites: an indicator of oxidation and implications for return samples from asteroids Ryugu and Bennu. Geochim. Cosmochim. Acta 303, 66–91. https://doi.org/10.1016/j.gca.2021.03.019.

Steller, T., Burkhardt, C., Yang, C., Kleine, T., 2022. Nucleosynthetic zinc isotope anomalies reveal a dual origin of terrestrial volatiles. Icarus 386, 115171. https://doi.org/10.1016/j.icarus.2022.115171.

Thomassin, D., Piani, L., Villeneuve, J., Caumon, M.-C., Bouden, N., Marrocchi, Y., 2023. The high-temperature origin of hydrogen in enstatite chondrite chondrules and implications for the origin of terrestrial water. Earth Planet. Sci. Lett. 616, 118225. https://doi.org/10.1016/j.epsl.2023.118225.

Weisberg, M.K., Kimura, M., 2012. The unequilibrated enstatite chondrites. Geochemistry 72 (2), 101–115. https://doi.org/10.1016/j.chemer.2012.04.003.

Wilke, M., Jugo, P.J., Klimm, K., Susini, J., Botcharnikov, R., Kohn, S.C., Janousch, M., 2008. The origin of S4+ detected in silicate glasses by XANES. Am. Mineral. 93 (1), 235–240. https://doi.org/10.2138/am.2008.2765.

Zolensky, M.E., Thomas, K.L., 1995. Iron and iron-nickel sulfides in chondritic interplanetary dust particles. Geochim. Cosmochim. Acta 59 (22), 4707–4712. https://doi.org/10.1016/0016-7037(95)00329-0.